Archives of Computational Methods in Engineering (2019) 26:1395–1413
https://doi.org/10.1007/s11831-018-9294-z

ORIGINAL PAPER

A Comprehensive Review of Computational Dehazing Techniques

Dilbag Singh[1] · Vijay Kumar[1]

Received: 8 February 2018 / Accepted: 12 September 2018 / Published online: 18 September 2018

Abstract
The visibility of outdoor images is greatly degraded due to the presence of fog, haze, smog etc. The poor visibility may cause the failure of computer vision applications such as intelligent transportation systems, surveillance systems, object tracking systems, etc. To resolve this problem, many image dehazing techniques have been developed. These techniques play an important role in improving performance of various computer vision applications. Due to this, the researchers are attracted toward the dehazing techniques. This paper carries out a comprehensive review of dehazing techniques to show that these could be effectively applied in real-life practice. On the other hand, it encourages the researchers to use these techniques for removal of haze from hazy images. The seven main classes of dehazing technique, such as depth estimation, wavelet, enhancement, filtering, supervised learning, fusion, meta-heuristic techniques and variational model are addressed. In addition, this paper focuses on mathematical models of dehazing techniques along with their implementation aspects. Finally, some considerations about challenges and future scope in dehazing techniques are discussed.

1 Introduction

With the advancements in computer vision applications, the dehazing techniques have gained the attention of researchers [159]. Dehazing techniques are extensively utilized in civil and military areas, such as target detection [27], traffic surveillance [24], remote sensing [128] etc. Therefore, the development of dehazing models have become a task of great interest and significance [31].

mn poor environmental conditions, illumination observed from a scene is sprinkled and immersed because of the considerable occurrence of molecules and aerosols are hanging in the environment [19]. With the worsening of environment eminence, fog phenomenon regularly happens [155]. Because of the effect of intense fog, haze or smog, the intelligibility of environment and visibility are becoming weak considerably that results in significant disturbance to different vision applications [59]. In poor environmental conditions, objects have poor visibility [161] and such images are often recognized as of low contrast and poor intensity [158].

Restoration of hazy image needs the information of physical features of the scene. One of these features is the depth of the scene [53]. It is evaluated from visual camera to the objects in the given scene. If depth of the scene is known, then the dehazing becomes much easier [36, 89]. However, depth map is unknown in prior for real-life applications [162]. Therefore, the fundamental problem in most of dehazing techniques is the accurate estimation of depth map [97]. The depth map estimation problem is not trivial and requires prior information of hazy image such as depth cues or atmospheric scattering [133]. The concept of depth map estimation is not new. It has been extensively utilized by artists to express depth to a viewer in their paintings as early as the renaissance[52]. Hazy imaging model has been studied and proved by various researchers such as Koschmieder [72] and McCartney [100].

Dehazing is a tough task because the transmission depends upon unknown depth which fluctuates according to weather conditions [60]. Tan et al. [76] and Kawakami et al. [67] restored hazy images by utilizing the local contrast values. These techniques are successful in segments which have significant weather gradient. However, the color of restored image is frequently over saturated [59]. The contrast maximization comes up with the over-saturation problem. The physics-based restoration techniques have an ability to overcome the over-saturation

✉ Dilbag Singh
dggill2@gmail.com

Vijay Kumar
vijaykumarchahar@gmail.com

[1] Thapar institute of engineering and technology, Patiala, Punjab 147001, India

problem [42]. He et al. designed a simple and effective dehazing technique using Dark channel prior (DCP) [59]. However, it suffers from halo artifacts and color distortion problems.

Dehazing techniques have made considerable improvements in recent times due to the utilization of efficient suppositions and priors [15]. Wang et al. [144] designed a patch-based DCP technique for solving this problem. But, it is worthless whenever the objects are intrinsically similar to airlight, and no shadow is directed on them [167]. The DCP has been found to be a well-organized restoration method in existing literature. However, its procedure may cause annoying halo and gradient reversal artifacts [171]. To handle these issues, several image filters have been developed to refine transmission map using a guided filter. However, these methods have high computational time [94]. To handle this problem, a filter has been designed using gain intervention [19]. However, it suffers from the gradient reversal artifacts and color distortion problem.

An adaptive DCP modelled by a Gaussian curve is designed which produces a more natural recovered image of sky and other bright regions [65]. It has better computational speed. However, the restored images may have halo artifacts. Yong et al. [34] implemented a novel dehazing technique that utilizes wavelet transform. The hazy image is divided into several spatial layers using the wavelet transform and then the restoration model is applied. It achieved high-quality results with good computational speed. But, it also suffers from the halo artifacts.

The soft matting based DCP is efficient for small size hazy images only. To overcome this issue, soft matting is replaced with an adaptively subdivided Quadtrees. The Quadtrees considerably decreased both computational time and storage space while still preserving the visual reliability of restored images [29]. But, these are not easy to scale. Zhao et al. designed a multi-scale tone technique to estimate the transmission map in an efficient manner. Therefore, it has ability to restore images by considering the different scales of hazy images [172]. But, it performs poorly for images which contain inhomogeneous haze.

Riaz et al. [120] improved dark channel by block and pixel level processing. The failure probability of DCP is reduced by utilizing the edge-preserving smoothing. But, it may introduce halo and gradient reversal artifacts [152]. Wang et al. [146] utilized Quadtree and gradient information to obtain the sky regions. These sky regions are filtered using Gaussian filter. This technique is best suitable for images with large haze gradients. However, it is unable to preserve the edges of restored image in efficient manner. The weighted estimation based dehazing technique can automatically improve a good atmospheric light.

The difference prior can monitor and remove the halo artifacts efficiently [124]. Fu et al. [45] improved image restoration process using DCP. This technique can remove the halo artifacts efficiently. But, [124] and [45] are unable to preserve significant edges of restored image. Image restoration from the perspective of noise filtering is designed. No refinement technique is required due to the pixel-wise noise monitoring. The saturated pixels problem can be easily removed using dehazing technique [94]. However, it also suffers from halo and gradient reversal problem

This paper has been structured as: Sect. 2 describes the haze imaging model. General framework and mathematical model of the DCP based dehazing techniques is discussed in Sect. 3. Section 4 describes the comprehensive review on existing well-known dehazing techniques along with their categorization. Challenges and future directions of dehazing techniques are described in Sect. 5. Section 6 describes different quality metrics which can be used to evaluate the performance of dehazing techniques. Comparative analysis based upon hardware and software used are discussed in the Sect. 7. In Sect. 8 significance and benefits to society of dehazing techniques are discussed. The concluding remarks and future scope are presented in Sect. 9.

2 Haze Imaging Model

The haze imaging model has been formulated by Koschmieder [72] and McCartney [100]. It is defined as:

$$I_s(m,n) = O_r(m,n)\gamma(m,n) + A_{tl}(1-\gamma(m,n)) \quad (1)$$

where I_s is the captured hazy image. O_r is actual object radiance. A_{tl} and γ indicate represent airlight and transmission map, respectively. (m, n) are pixel coordinates of an image. Figure 1 indicate the haze imaging model for

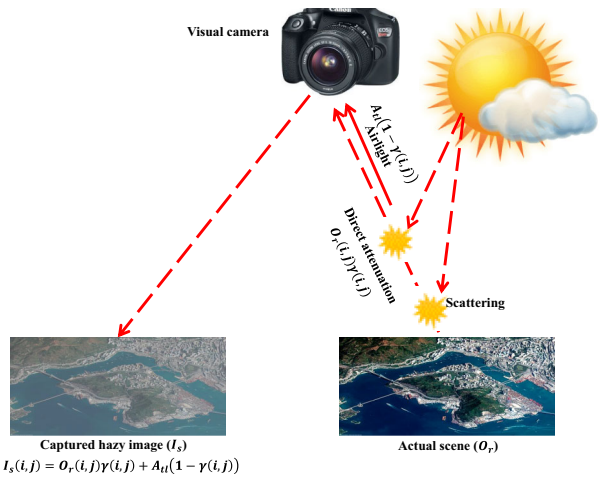

Fig. 1 Haze imaging model

remote sensing images. The γ shows the light which is not sprinkled and received by visual sensor [26].

The transmission map (γ) is computed as [59]:

$$\gamma(m,n) = exp^{-s_{cf}(m,n)D(m,n)} \tag{2}$$

where $D(m, n)$ is distance between scene and visual sensor. $s_{cf}(m,n)$ is the sprinkling factor that relies on wavelength (λ) and turbidity (t_d). In hazy environment, $s_{cf}(m,n)$ is generally assumed to be independent of wavelength. $\gamma \in [0, 1]$ [153].

3 Dark Channel Prior Based Dehazing

From the existing study, it has been observed that the dehaze based upon DCP has five steps (see Fig. 2). These steps are DCP, airlight estimation, transmission map estimation, coarse estimated atmospheric veil estimation and restoration model. The mathematical formualtion of these steps are as follows:

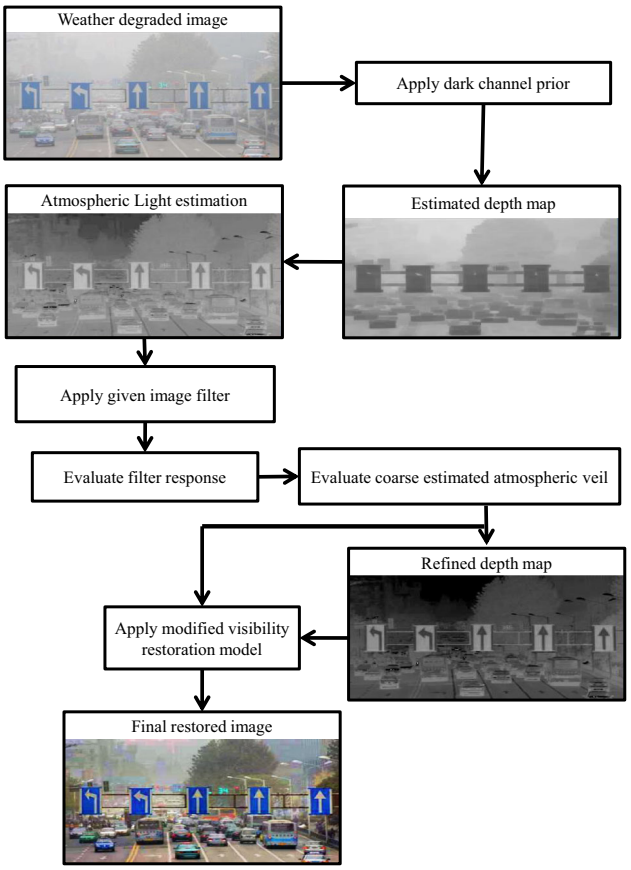

Fig. 2 Dehazing model

3.1 Dark Channel Prior

The DCP states that at least one-color channel (i.e., red, green, or blue) contains some pixels whose pixel values approaches to 0. The minimum pixel value in such a patch is 0. For O_r, DCP is defined as:

$$\Updownarrow^{d}(m,n) = \min_{y\in\Omega(m,n)} \left(\min_{c\in(r,g,b)} \left(I_s^c(l)\right)\right) \tag{3}$$

Here, I_s^c is the available color channels of I_s. $\Omega(m,n)$ shows the local mask at coordinates (m, n).

3.2 Airlight Estimation

From Eq. (1), it has been observed that the airlight is extra dominant as the distance from scene to visual camera increases. Image dehazing model shows that two scenes with different radiant energy, located at same distance from the camera, have similar airlight. Airlight (A_{tl}) is evaluated in most of the hazy-opaque regions [105].

The value of A_{tl} is evaluated from I_s, from similar regions as its depth image. Pixel with maximum luminance in I_s is known as the global atmospheric light. Pixel with highest dark channel value is considered to estimate A_{tl}. It is evaluated as [59]:

$$A_{tl}(m,n) = I_s\left(\max_c\left(I_s^c\right)\right). \tag{4}$$

3.3 Transmission Map Estimation

To estimate the transmission map (γ), I_s is normalized by A_{vl}. Assume that the A_{vl} is known. Therefore, Eq. (1) is rewritten as:

$$\frac{m_s(m,n)}{A_{tl}} = \frac{\gamma(m,n)O_r(m,n)}{A_{tl}} + 1 - \gamma(m,n) \tag{5}$$

Assume that the transmission in local mask ($\Omega(m,n)$) be constant. The mathematical formulation of transmission is given by $\bar{\gamma}(m,n)$. Apply DCP on both sides of Eq. (5). In the same way, minimum operators are applied on both sides as:

$$\begin{aligned} &\min_{y\in\Omega(m,n)}\left(\min_c \frac{m^c(y)}{A_{tl}^c}\right) \\ &= \tilde{\gamma}(m,n)\min_{y\in\Omega(m,n)}\left(\min_c \frac{O_r^c(y)}{A_{tl}^c}\right) + 1 - \tilde{\gamma}(m,n) \end{aligned} \tag{6}$$

where $\gamma(m,n)$ is a constant value. Thus, $\gamma(m,n)$ can be placed outside of the minimum operators. The DCP of $O_r \to 0$, it is defied by $O^{\mathrm{d}}(m,n)$. The mathematical formulation of $O^{\mathrm{d}}(m,n)$ is as:

$$O^{\mathrm{d}}(m,n) = \min_{y\in\Omega(m,n)} \left(\min_{c} O_r^c(y) \right) = 0 \tag{7}$$

As $A_{tl}^c \in \mathbb{R}$, that results in:

$$\min_{y\in\Omega(m,n)} \left(\min_{c} \frac{O_r^c(y)}{A_{tl}^c} \right) = 0 \tag{8}$$

Generally, $\min_{y\in\Omega(m,n)} \left(\min_{c} \frac{O_r^c(y)}{A_{tl}^c} \right)$ is the DCP of normalized hazy image $\frac{O_r^c(y)}{A_{tl}^c}$. $\tilde{\gamma}(m,n)$ id defined as:

$$\tilde{\gamma}(m,n) = 1 - \min_{y\in\Omega(m,n)} \left(\min_{c} \frac{m_s^c(y)}{A_{tl}^c} \right) \tag{9}$$

It has been observed that the DCP performs poorly for sky regions. Because, the color of sky in a I_s is identical to A_{tl}. Therefore, $\min_{y\in\Omega(m,n)} \left(\min_{c} \frac{m^c(y)}{A_{tl}^c} \right) \to 1$. Thus, $\bar{\gamma} \to 0$. The estimated transmission map [Eq. (9)] has ability to handle sky and non-sky regions. Thus, isolation of sky regions is not required.

The presence of haze is an necessity indication for human to observe depth so called aerial perspective. If we remove haze completely, then the dehazed image seems like artificial image. Thus, some amount of haze is allowed for distant objects using a constant attribute $\beta \in [0,1]$. Therefore, Eq. (9) is redefined as:

$$\tilde{\gamma}(m,n) = 1 - \beta \min_{y\in\Omega(m,n)} \left(\min_{c} \frac{m_s^c(y)}{A_{tl}^c} \right) \tag{10}$$

3.4 Coarse Atmospheric Veil Estimation

Initially, the coarse estimated atmospheric veil ($A_{viel}(m,n)$) is computed as [19, 29, 137]:

$$A_{viel}(m,n) = 1 - \gamma(m,n) \tag{11}$$

From Eqs. (10) and (11), the normalized value of $A_{viel}(m,n)$ is computed as:

$$A_{viel}(m,n) = \beta \min_{y\in\Omega(m,n)} \left(\min_{c} \frac{m_s^c(y)}{A_{tl}^c} \right) \tag{12}$$

The estimation of $A_{viel}(m,n)$ has been done by considering the minimum operation of object $\frac{m_s(m,n)}{A_{tl}}$. It will results in $A_{viel}(m,n)$'s discontinuity even if no unexpected depth discontinuities occur. To overcome the effect of halo artifacts, an efficient image filter is required to refine the $A_{viel}(m,n)$.

The trilateral filter based coarse estimated atmospheric veil estimation is considered for understanding purpose. From [137] and [123], $A_{viel}^c(m,n) = A_{tl}(1 - \gamma(m,n))$ is set as the transmission veil, $\gamma(m,n) = \min_c(I_s^c(m,n))$ is the minimum color channel of $I_s(m,n)$. The value of $A_{viel} \in [0\ \gamma]$. Therefore, it does not affect gray images. By applying the filter, transmission refinement is computed as:

$$\bar{\gamma}(m,n) = var(m,n) - J_O^{tf}\Big(|\gamma - var(m,n)|\Big) \tag{13}$$

where $var(m, n)$ is the variance of pixel centered at position (m, n).

Assume that I_{val} and G_{val} be illuminate values at pixel q of minimum channel object and guided image, respectively. K_r is kernel mask at (m, n). The G_d is guided image. The trilateral filter (J_O^{tf}) is defined as:

$$J_O^{tf}(I_s) = \frac{\left(\sum_{q\in k_r} \gamma^{pq}(G_d) \times I_q \times var(I_q, G_d) \right)}{\sum_{q\in K_r} \gamma^{pq}(G_d)} \tag{14}$$

Here, $\gamma^{pq}(G_d)$ is the kernel weight and evaluated as:

$$\gamma(G_d) = \frac{1}{|n|^2} \sum_{n:(p,q)\in k_r} \left(1 + \frac{(G_{dp} - \mu_n)(G_{dq} - \mu_n)}{\sigma_n^2 + \epsilon} \right) \tag{15}$$

Here, μ_n and σ_n^2 are mean and variance of G_d in local patch (k_r), respectively. $|n|$ shows the number of pixels in patch. When G_{dp} and G_{dq} are on similar side of an edge, then the weight assigned to pixel (q) is maximum. When G_{dp} and G_{dq} are on different sides, then the minimum weight will be allocated to q.

3.5 Haze Restoration Model

The primary goal of restoration model is to restore O_r from I_s. It has been observed that A_{tl} requires to be specified and γ as input prior. O_r is evaluated as [59]:

$$O_r(m,n) = \frac{m_s(m,n) - A_{tl}}{\gamma(m,n)} + A_{tl} \tag{16}$$

The O_r suffers from noise when $\gamma \to 0$. γ is constrained as a lower bound by γ_l. According to related work, γ_l is taken to be 0.1 [59]. Therefore, O_r is rewritten as:

$$O_r(m,n) = \frac{m_s(m,n) - A_{tl}}{\max(\gamma(m,n), \gamma_l)} + A_{tl} \tag{17}$$

4 Dehazing Techniques

This section contains comprehensive review on existing well-known dehazing techniques. The categories of image restoration techniques are shown in Fig. 3. The dehazing techniques are categorized into seven main categories. These are (1) Depth estimation based dehazing, (2) Wavelet based dehazing, (3) Enhancement based dehazing (4) Filtering based dehazing, (5) Supervised learning based dehazing, (6) Fusion based dehazing and (7) Meta-heuristic

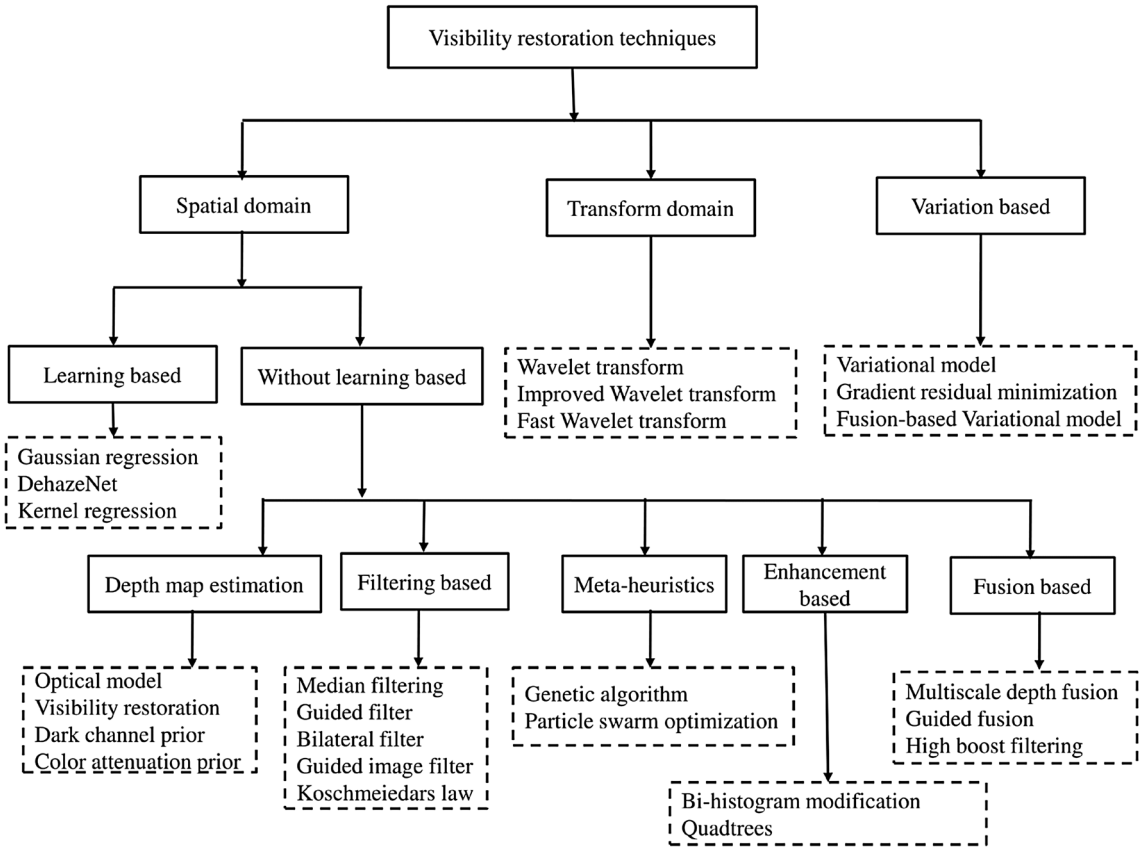

Fig. 3 Image restoration techniques

techniques based dehazing. The subsequent section contains the details of various dehazing techniques along with their strengths and weaknesses.

4.1 Depth Estimation Based Dehazing

Majority of existing image dehazing techniques are based upon the depth map estimation techniques [172]. Initially, depth of image is evaluated by considering some assumptions or priors. Based upon evaluated depth map, transmission map and atmospheric veil will be evaluated [21, 50, 83]. The performance of depth map estimation techniques purely depends upon the used assumptions. Mostly, these methods suffer from various issues such as the sky-region, edge degradation, color distortion, Gradient reversal artifacts, Halo artifacts etc. [145].

Table 1 shows the comparison of existing techniques based upon certain features and artifacts. In Table 1, Edge preservation, Speed, Color distortion, Halo artifacts, Large haze gradient, Gradient reversal artifacts and Blocking artifacts are written as EP, S_P, HA, LHG, GRA and BA, respectively.

Table 2 shows some well-known restoration techniques used that have been used for depth map estimation along with their mathematical formulations. The comparisons have been done by considering prior such as Background light (BL) and Transmission map (TM). In Table 2, (m, n) denotes the coordinates of the pixel. $I_s^c(m,n)$ shows the hazy image. $O_r(m,n)$ represents the actual scene radiance. A_{tl} and $\gamma(m,n)$ represents background light and transmission map, respectively. $D(m, n)$ demonstrates distance between visual camera and given object. β^c represents spectral volume attenuation coefficient for channel c. $\Omega(m,n)$ demonstrates the square local patch centered at x. $p_{0.1\%}$ denotes the set of positions of top 0.1% brightest pixels in $I_s^c(m,n)$. $\widetilde{A_{tl}}$ and $\gamma(\widetilde{m,n})$ represent the estimated BL and estimated TM of each channel. $D_{mip}(m,n)$ represents closer scene points whose red light attenuates less than that of farther scene points. P_{blr} denotes the refined blurriness map. F_s represents the soft matting. Here, $c \in r, g, b$ and $c' \in g, b$.

4.2 Wavelet Based Dehazing

To improve the speed of restoration techniques and to reduce color distortion, transform based restoration techniques have been introduced. When a hazy image is restored by converting it into time, frequency or wavelet

Table 1 Comparative analysis of depth map dehazing techniques

References	Year	EP	S_P	CD	HA	LHG	GRA	BA
[71]	2008	✓	Average	✓	×	×	✓	×
[134]	2008	✓	Average	✓	✓	×	×	✓
[137]	2009	×	Good	✓	×	×	×	×
[137]	2009	×	Good	✓	×	×	×	×
[73]	2009	×	Good	×	✓	✓	✓	✓
[155]	2010	×	Good	✓	×	×	×	×
[59]	2011	×	Average	✓	×	×	×	×
[59]	2011	✓	Average	×	✓	✓	×	×
[108]	2012	×	Good	✓	×	×	×	×
[13]	2012	×	Good	✓	×	×	×	×
[101]	2013	×	Average	×	✓	✓	✓	✓
[131]	2013	×	Average	✓	×	×	×	×
[160]	2013	×	Good	×	✓	✓	✓	✓
[43]	2014	×	Average	×	×	×	×	×
[96]	2014	✓	Average	×	✓	✓	×	×
[49]	2014	×	Good	×	✓	✓	✓	✓
[21]	2015	✓	Average	×	×	✓	✓	✓
[87]	2015	✓	Good	×	×	×	✓	✓
[45]	2015	×	Good	×	✓	✓	×	✓
[142]	2015	✓	Average	×	✓	✓	×	×
[165]	2015	✓	Average	×	×	✓	✓	✓
[75]	2015	×	Good	×	✓	✓	✓	✓
[177]	2015	✓	Average	×	×	✓	✓	✓
[145]	2016	×	Average	×	✓	✓	×	✓
[17]	2016	×	Good	×	✓	✓	×	✓
[66]	2016	×	Good	×	✓	✓	×	✓
[119]	2016	✓	Average	×	×	✓	✓	✓
[166]	2017	✓	Average	×	✓	✓	×	×
[147]	2017	×	Good	×	✓	✓	×	✓
[168]	2017	✓	Average	✓	✓	×	✓	✓

domains with a pair of mathematical operations called a transform domain-based restoration [121, 163]. However, these techniques may introduce certain color artifacts in the restored images. Also, these techniques have poor computational speed. To overcome this issue modified dehazing techniques have proposed in the literature [69, 149]. These techniques utilizes wavelet and DCP to improve the quality of restored images.

Liu et al. [95] used correlative relationship of wavelet approach to remove the effect of haze and enhance the texture simultaneously. Qiao et al. [116] utilized contrast limited adaptive histogram equalization and wavelet transform to improve the quality of underwater images. To distinguish between noise and useful information of image, the soft threshold method is used. Song et al. [129] used Particle Swarm Optimization (PSO) and Genetic Algorithm (GA) with fuzzy logic to dehaze the image. Zhang et al. [170] implemented an algorithm to estimate the atmospheric light using ACO (Table 3).

4.3 Enhancement Based Dehazing

Image enhancement techniques such as Histogram Equalization [44], Weighted Histograms [61], Bi-histogram modification [18], Histogram modification [51] etc. have been extensively utilized to remove the haze from hazy images. However, technique techniques suffer from over/under enhancement issues and saturation pixels issues. Also, these approaches work inefficiently for images with large haze gradient or when images contain inhomogeneous haze (Table 4).

4.4 Filtering Based Dehazing

To refine the coarse estimation atmospheric veil, various filters have been used such as median filter [75], L2-norm with guided filter [30], Weighted guided image filter [88], Bilateral filter [132], Weighted guided image filter and Koschmiedars law [86]. However, filtering based methods suffer from computational speed issue. Also, these methods completely depend upon the estimation performance of various priors (Table 5).

4.5 Supervised Learning Based Dehazing

Estimation of depth map in an efficient manner is still an open area of research. Because estimation of depth map depends upon certain assumptions. Therefore, recently researchers have started using machine learning models to evaluate the depth map in a more efficient manner. These technique are as Linear model [177], Two-layer Gaussian regression [38], DehazeNet [12], Kernel regression model [156] etc. However, a lot of hazy and haze free images of the dissimilar scenes are required to train a given model that make it difficult for real-time implementation (Table 6).

4.6 Fusion Based Dehazing

Image fusion is found to be another interesting and efficient technique to remove the haze from images [148]. Riaz et al. implemented a guided fusion-based depth map estimation tehnchnique. It effectively decreases the failure possibility of DCP and restoration artifacts. DCP failure in brighter segments by decreasing the contrast of brighter segments. Therefore, it provides an even more natural restoration of the brighter segments [120].

Image regions that have low light intensity and dense haze still gets affected adversely with lesser visibility. In

Table 2 Formulas for estimation of depth, airlight, and transmission map in image restoration methods

References	Prior (I_s^c)	BL estimation ($\widetilde{A_{tl}}$)	TM estimation ($\tilde{\gamma}$)
[16]	I_s^d	$I_s^c(\max_{m,n}\ p(m,n))$	$\tilde{\gamma}(m,n) = 1 - \min_c\big(\min_{y\in\Omega(m,n)} I_s^c(y)\widetilde{A_{tl}}\big)$
[14]	D_{mip}	$I_s^c(\max_{m,n}\ \tilde{\gamma}(m,n))$	$\tilde{\gamma}(m,n) = D_{mip} + \big(1 - \max_{m,n} D_{mip}(m,n)\big)$
[161]	I_s^d	$I_s^c(\max_{m,n\in p_{0.1\%}}(\sum_k I_s^c(m,n)))$	$\tilde{\gamma}(m,n) = 1 - \min_c\big(med_{y\in\Omega(m,n)}\frac{m_s^c(y)}{\widetilde{A_{tl}}}\big)$
[22]	I_s^d	$I_s^c(\max_{m,n}\ I_d^c(m,n))$	$\widetilde{\gamma^r}(m,n) = 1 - \min_c\big(\min_{y\in\Omega(m,n)}\frac{m_s^c(y)}{\widetilde{A_{tl}}}\big),\ \widetilde{\gamma^{c'}} = (\widetilde{\gamma^r})^{\frac{\beta^{c'}}{\beta^r}}$
[151]	$I_{c'}^d$	$I_s^c\Big(\min_{m,n}\Big(I_d^r(m,n) - \max_{c'}(I_d^{c'}(m,n))\Big)\Big)$	$\widetilde{\gamma^{c'}}(m,n) = 1 - \min_{c'}\big(\min_{y\in\Omega(m,n)}\frac{m_s^{c'}(y)}{\widetilde{A_{tl}^{c'}}}\big),\ \widetilde{\gamma^r} = (\tau \max_{y\in\Omega(m,n)} I_s^r(y),$ $\tau = \frac{avg_{m,n}(\widetilde{\gamma^{c'}}(m,n))}{avg_{m,n}\big(\max_{y\in\Omega(m,n)} I_s^r(y)\big)}$
[33]	$I_{c'}^d$	$I_s^c(\max_c\ p(m,n))$	$\tilde{\gamma}(m,n) = 1 - \min_c\big(\min_{y\in\Omega(m,n)}\frac{m_s^c(y)}{\widetilde{A_{tl}}}\big)$
[46]	$I_{r'c'}^d$	$I_s^c(\min_{m,n\in p_{10\%}} I_d^r(m,n))$	$\tilde{\gamma}(m,n) = 1 - \min\Big(\frac{\min_{y\in\Omega(m,n)}(1-I_s^r(y))}{1-\widetilde{A_{tl}^r}}, \frac{\min_{y\in\Omega(m,n)} I_s^g(y)}{\widetilde{A_{tl}^g}}, \frac{\min_{y\in\Omega(m,n)} I_s^b(y)}{\widetilde{A_{tl}^b}}\Big)$
[173]	I_s^d	$I_s^c\Big(\max_{m,n\in p_{0.1\%}}\big\lvert I_d^r(m,n) - I_d^{c'}(m,n)\big\rvert\Big)$	$\widetilde{\gamma^r}(m,n) = 1 - \min_c\Big(\min_{y\in\Omega(m,n)}\frac{m_s^c(y)}{\widetilde{A_{tl}}}\Big),\ \widetilde{\gamma^{c'}} = (\widetilde{\gamma^r})^{\frac{\beta^{c'}}{\beta^r}}$
[115]	$1 - P_{blr}$	$\frac{1}{p_{0.1\%}}\sum_{m,n\in p_{0.1\%}} I_s^c(m,n)$	$\tilde{\gamma}(m,n) = F_s\big(P_{blr}(m,n)\big)$

Table 3 Comparative analysis of wavelet based restoration techniques

References	Year	EP	S_P	CD	HA	LHG	GRA	BA
[34]	2002	×	Average	✓	×	×	×	×
[22]	2012	×	Good	×	×	✓	×	×
[121]	2014	✓	Good	×	×	×	×	×
[129]	2014	×	Average	×	×	×	×	×
[69]	2017	×	Good	✓	×	×	×	×
[116]	2017	×	Good	×	×	×	×	×
[95]	2017	×	Good	×	×	✓	×	×
[170]	2017	×	Average	✓	×	×	×	×

Table 4 Comparative analysis of enhancement based restoration techniques

References	Year	EP	S_P	CD	HA	LHG	GRA	BA
[4]	2010	✓	Average	✓	✓	×	✓	✓
[3]	2013	✓	Average	×	✓	×	✓	×
[151]	2013	×	Average	✓	×	×	✓	✓
[149]	2014	×	Average	✓	×	×	×	×
[62]	2014	×	Average	×	×	×	×	×
[18]	2015	×	Good	×	×	✓	×	×
[173]	2015	×	Good	✓	×	×	✓	×
[115]	2015	✓	Average	×	✓	×	✓	×
[102]	2016	×	Good	✓	×	×	✓	×
[7]	2016	✓	Average	×	✓	×	×	×
[82]	2016	✓	Average	×	✓	×	×	×
[128]	2017	✓	Good	✓	✓	×	✓	✓
[157]	2017	✓	Average	×	✓	×	✓	×
[118]	2017	×	Average	✓	×	×	✓	✓
[175]	2017	×	Good	✓	×	×	✓	×
[51]	2017	✓	Average	×	✓	×	✓	×

[42], the techniques which deal with contrast improvement on a global level are studied. The effect of haze on the image objects is depends upon its varying intensity and color contrast of the pixels. Now, there is a family of contrast enhancement schemes which can be applied on the whole image. Thus, this limitation in general provides over/under saturated images. The white balance, histogram equalization and gamma correction are the examples of popular image enhancement operators.

To fix this limitation, the fusion-based restoration technique has considered three different measures. It uses the weight maps. They take pixels into consideration and define customized spatial functions for poor contrast regions.

Luminance weight map calculates pixel visibility of an image and assign values proportional to their visibility. For

Table 5 Comparative analysis of filter based restoration techniques

References	Year	EP	S_P	CD	HA	LHG	GRA	BA
[70]	2013	✓	Average	×	×	×	×	×
[123]	2014	✓	Good	×	×	×	×	×
[88]	2015	✓	Good	×	✓	×	×	×
[86]	2015	✓	Average	×	✓	✓	×	×
[18]	2015	✓	Good	×	✓	✓	✓	✓
[15]	2015	×	Average	×	✓	×	✓	✓
[94]	2016	✓	Average	×	✓	✓	✓	✓
[19]	2016	×	Average	×	✓	✓	✓	×
[99]	2016	✓	Good	×	✓	✓	✓	✓
[64]	2017	✓	Average	×	✓	✓	✓	✓
[93]	2017	×	Good	×	✓	✓	×	✓
[126]	2017	✓	Good	✓	✓	✓	✓	✓
[127]	2017	✓	Good	✓	✓	✓	✓	✓

Table 6 Comparative analysis of learning based restoration techniques

References	Year	EP	S_P	CD	HA	LHG	GRA	BA
[29]	2013	✓	Good	×	×	×	×	×
[135]	2014	×	Average	×	✓	✓	×	×
[143]	2015	×	Good	×	✓	✓	×	×
[112]	2015	✓	Average	×	✓	×	×	×
[83]	2015	✓	Average	×	×	✓	×	×
[50]	2015	×	Good	×	✓	✓	×	×
[12]	2016	✓	Average	×	✓	×	×	×
[156]	2016	✓	Good	×	✓	✓	✓	×
[38]	2016	✓	Good	×	✓	✓	×	✓
[98]	2016	✓	Good	×	✓	✓	✓	×

hazy images, color loss is calculated based upon RGB information as they have low saturation in general. Let R, G, B and L are colors and luminance intensities for each input image with index n. The weight is calculated as [120]:

$$W_n^L = \frac{1}{\sqrt{3}}\sqrt{(L^n - R^n)^2 + (L^n - G^n)^2 + (L^n - B^n)^2} \quad (18)$$

Luminance is calculated from the average of RGB intensities. Hence, the restored regions will yield greater value of W^L. Thus, W^L is an index for degradation identification due to haze effect.

Hazy image is white balanced to obtain I_1 [10]. Then, I_2 is obtained by taking the scaled difference of illumination value of the image (pixels) and its average luminance (I_{avg}). I_2 is mathematically computed as:

$$I_2 = \alpha(I - I_{avg}) \quad (19)$$

The derived weighted luminance helps a smooth transition among derived input images (I_1, I_2). To reduce the global color and contrast, two additional weighted maps based upon chromaticity and saliency are defined as:

$$W_n^C = exp\left(\frac{(S_n - S_{max})^2}{-2\sigma^2}\right) \quad (20)$$

W^C calculates the squared difference in saturation value and its maximum value. The default value for our experiments σ and S_{max} are set to 0.3 and 1, respectively. Thus, the value is proportional to the saturation of the pixel values. Therefore, the saturation regions are better form the outcome.

Saliency weighted map calculates the visibility degree relative to the neighborhood areas. It basically measures the relative contrast of a region or a segment in an image with respect to its surroundings. It is based upon neighboring orientation, color or intensities.

The saliency weight map is defined as [1]:

$$W_n^S = \|I_n^f - I_n^{avg}\| \quad (21)$$

Here, I_n^{avg} is the average pixel value of input I_n and I_n^{avg} is the blurred input. It is obtained by using high frequency value of cutt-off ($f = \pi/2.75$) into a separable binomial kernel. Binary kernel is efficient to compute for small kernels if calculated in this way with $5 \times 5(1/16)[14641]$. This approach yields uniform contrast regions with well-separated boundaries while preventing unnecessary artifacts in the fused image. The impact of three measures are important in different aspects but the first one which is luminance weight map, has greater visibility impact overall. The aggregated weight map (W_n) is obtained by multiplicative expression:

$$W_n = W_n^L \times W_C^n \times W_n^S \quad (22)$$

The normalized form of aggregate weight to guarantees that the sum will be equal to 1 for each pixel:

$$\overline{W}_n = \frac{W_n}{\sum W_n} \quad (23)$$

During the image fusion, weighted inputs are computed in order to detect the features more significantly for each pixel

$$F = \sum_n \overline{W}_n I_n \text{s.t.} \sum_n \overline{W}_n = 1 \quad (24)$$

Intensity scale of the resulted image is maintained because normalized weighted map is used in the above calculation. But, this equation may result in halo artifacts where the weighted maps have stronger transitions. Therefore, an

approach [11] which is known as pyramidal refinement is implemented to get rid of this degradation.

In this technique, I_n is actually decomposed using Laplacian operator into a pyramid with different scales. On the parallel track, $\overline{W}_n$ is also derived to a Gaussian pyramid for each of its weighted normalized map. At each respective pyramid level m the mixing is applied as:

$$F_m = \sum_n G_m(\overline{W}_n) L_m(I_n) \tag{25}$$

Here, L_m shows Laplacian operation of m. $G_m(\overline{W}_n)$ is the Gaussian operator on the weighted normalized map $\overline{W}_n$. Bottom up direction is adopted for respective pyramid layers and the final restored version of m is calculated after adding all the pyramid levels using upsampling operator $U(x)$ with $x = 2^{m-1}$.

$$G(x) = \sum_m F_m(x) U(x) \tag{26}$$

In the fusion based restoration method, all three weights have equal weighted contribution towards the results of final fusion .

A fusion strategy based dehazing technique is implemented in [99], which fuses the outcomes of the linear transform with the guided image filtering. It not only improves the visibility of images at good computational speed (Table 7).

4.7 Meta-heuristic Techniques Based Dehazing

Parameter tuning of dehazing techniques is found to be challenging issue in the literature. It has been concluded that the efficient tuning of parameters such as white balancing factor, patch size, restoration value etc. have an ability to improve the overall performance of existing dehazing techniques [94]. Guo et al. implemented genetic algorithm based dehazing technique to optimize depth map evaluated using DCP. However, genetic algorithm suffers from pre-mature convergence and poor convergence speed issues [54]. Song et al. [129] used Particle Swarm Optimization (PSO) and Genetic Algorithm (GA) with fuzzy logic to restore the visibility of degraded images. Zhang et al. [170] designed an algorithm to estimate the atmospheric light using Ant Colony Optimization (ACO) (Table 8).

Table 7 Comparative analysis of fusion based restoration techniques

References	Year	EP	S_P	CD	HA	LHG	GRA	BA
[4]	2010	×	Average	✓	✓	✓	×	×
[3]	2013	×	Average	✓	✓	×	×	✓
[148]	2014	✓	Average	×	✓	✓	×	×
[169]	2014	✓	Average	✓	×	×	✓	✓
[120]	2016	✓	Good	×	✓	✓	×	✓
[102]	2016	✓	Average	✓	✓	×	×	✓
[99]	2016	×	Average	×	✓	×	✓	✓
[150]	2016	×	Good	✓	✓	✓	×	✓
[136]	2017	✓	Average	×	✓	✓	✓	×
[5]	2017	×	Average	✓	✓	✓	×	×

4.8 Variational Image Restoration

The depth map estimation techniques are face failure whenever the physical assumptions are violated. Enhancement based dehazing techniques suffer from over/under enhancement issues. Also, not effective for images with large haze gradients. To overcome these issues, recently variational based image dehazing techniques have been designed [47].

To restore haze-degraded outdoor images, the enhanced variational image-dehazing (EVID) energy minimization function has been designed. It is computed as [47]:

$$\begin{aligned} E_{\text{EVID}}(m_s^c) = {} & \frac{\alpha}{2}\sum_m (m^c(i) - \mu^c)^2 + \frac{\beta}{2}\sum_m (m^c(i) - m_0^c(i))^2 \\ & - \frac{\gamma}{2}\sum_{m,n} \omega(m,n)|m^c(i) - m^c(j)| \\ & - \frac{\eta}{2}\sum_{m,n} \omega(j,j)|m^c(i) - m^{c+1}(j)| \\ & - \frac{\eta}{2}\sum_{m,n} \omega(m,n)|m^c(i) - m^{c+2}(j)| \end{aligned} \tag{27}$$

Here, I_s^c represents the color channel $\in [0,1]$. I_0 represents the input image with m and n pixel coordinates. α, β, γ and η are positive constants. $\omega(m,n)$ is a distance parameter whose values are decreased as the distance between m and n is increased. ^{c} represents the predicted mean of the haze-free image; and $c \in \mathbb{Z}_3$.

Recently, many variational image dehazing models have implemented by Fang et al. [39], Galdran et al. [47], Chen et al. [20] and Galdran et al. [48]. However, these technique suffer from poor computational speed.

Table 8 Comparative analysis of meta-heuristic based restoration techniques

References	Year	EP	S_P	CD	HA	LHG	GRA	BA
[129]	2014	×	Average	×	✓	✓	×	×
[55]	2016	✓	Average	×	✓	✓	✓	×
[63]	2016	✓	Average	×	✓	×	✓	×
[174]	2017	✓	Average	×	✓	✓	✓	×
[170]	2017	✓	Average	✓	×	✓	×	✓

Table 9 Comparative analysis of variational model based restoration techniques

References	Year	EP	S_P	CD	HA	LHG	GRA	BA
[39]	2010	✓	Average	×	✓	✓	✓	×
[47]	2015	✓	Average	✓	✓	✓	✓	×
[141]	2015	✓	Average	×	✓	✓	✓	✓
[164]	2016	✓	Average	×	✓	✓	✓	×
[20]	2016	✓	Average	✓	✓	✓	✓	×
[140]	2017	✓	Average	×	✓	✓	✓	✓
[48]	2017	✓	Average	✓	✓	✓	✓	✓

Table 9 shows the comparative analysis between variational based dehazing techniques. It has been observed that these techniques provide efficient results as compared to other existing techniques. However, these techniques are suffered from poor computation speed.

4.9 Comparative Analysis

Table 10 shows the comparison of Depth estimation (DE), Multi-images (MI), Polarizing filter (PF), Known depth (KD) and Single image (SI) based dehazing techniques by considering the attributes known in prior. In this table, $I_{g2}(m,n)$ depicts two gray images with different scattering coefficients $\beta 1$, $\beta 2$. $\gamma(m,n)$ represents transmission map. d_p represents depth map. A_{tl} depicts atmospheric light. $I^c(m,n)$ shows single color image. $I_2^c(m,n)$ with different weather conditions ($\beta 1$, $\beta 2$).

The dehazing techniques can be divided into two categories such as which require mathematical model and which do not require mathematical model. Here, KD and MI do not need any mathematical model to calculate the depth information for images. As required information is available along with the hazy image. Also, DE, PF and SI are examples of mathematical based restoration techniques.

5 Challenges

Designing an efficient image dehazing technique is still an ill-posed problem [130, 154]. Dehazing of images depends upon certain assumptions that result in halo artifacts, color distortion, edge degradation etc. [6, 78]. Therefore, the main goal of dehazing techniques are to restore color and significant details hazy images [32, 41, 80, 92]. By studying the existing dehazing techniques [84, 91, 110, 138], it has been observed that following are the main issues that needs to be handled in the future.

5.1 Atmospheric Light Monitoring

The atmospheric light can be efficiently calculated with the help of DCP, particularly when dark channel utilizes large local mask. However, it has been observed that larger mask size provides over smooth depth map, that causes the over-saturation problem. Also, smaller size may introduce certain restoration artifacts such as halo, gradient reversal artifacts, etc. [79].

5.2 Saturated Pixels

Saturation of pixels is found to be critical problem with existing dehazing techniques. It means that some of the pixels which were not black or white become white or black after applying the dehazing process.

5.3 Large Haze Gradient

Majority of existing techniques perform significantly for images with low haze. However, these techniques lose significant details of restored images with large haze gradient

5.4 Parameter Tuning

An efficient tuning of parameters has ability to improve the performance of existing dehazing techniques. However, parameters of existing dehazing techniques have been taken manually or by doing some experiments. It limits the performance of the existing dehazing techniques. Because adaptive selection of these parameters has ability to improve the performance of these techniques. Meta-heuristics techniques-based optimization techniques have ability to handle this issue in an efficient manner.

6 Performance Metrics

This section briefly discusses various performance metrics used to analyze the performance of dehazing techniques. Figure 4 shows various performance metrics that have been used in literature to evaluate the performance of dehazing techniques [37, 51, 114]. These metrics are categorized into two parts i.e., when ground truth images are available and when ground truth image are not available [18, 109]

6.1 When Ground Truth Images are Given

In this category, a ground truth image (reference image) is available. Many performance metrics have been implemented by various researchers such as Structural Similarity

Table 10 An overview of existing works on vision through atmospheric scattering media

References	Type	Attribute(s) known in prior	Attribute(s) going to be estimated	Key principle
[176]	DE[b]	$I_g(m,n)$ and $O_r(m,n)$	$t(m, n)$ and $d_p(m,n)$	Direct solving
[107]	DE[b]	I_{g2}	$t(m, n)$ and $d_p(m,n)$	Comparing different β
[172]	DE[b]	$I_g(m,n)$ and A_{tl}	$t(m, n)$ and $d_p(m,n)$	Direct solving
[104]	DE[b]	$I^c(m,n)$	$t(m, n)$, $d_p(m,n)$ and A_{tl}	Dichromatic model
[103]	MI[a]	$I_2^c(m,n)$	$t(m, n)$, $d_p(m,n)$	Colour decomposition
[105]	MI[a]	$I^{g2}(m,n)$ and $I_2^c(m,n)$	$\gamma(m,n)$, $d_p(m,n)$, A_{tl} and $O_r(m,n)$	Color decomposition
[13]	MI[a]	Stereo Cameras	$d_p(m,n)$ and $O_r(m,n)$	Depth from scattering; Depth from stereo images
[87]	MI[a]	Monocular video	$\gamma(m,n)$, $d_p(m,n)$ and $O_r(m,n)$	Depth from monocular video; Depth from scattering
[122]	PF[b]	$I^{g2}(m,n)$ and $I_2^c(m,n)$	A_{tl}, $\gamma(m,n)$, $d_p(m,n)$ and $O_r(m,n)$	Assuming $d_p(m,n)$ has insignificant polarization
[125]	PF[b]	$I^{g2}(m,n)$ and $I_2^c(m,n)$	A_{tl}, $\gamma(m,n)$, $d_p(m,n)$ and $O_r(m,n)$	A_{tl} and $d_p(m,n)$ are statistically independent
[111]	KD[a]	$I_g(m,n)$ and $d_p(m,n)$	A_{tl}, β and $O_r(m,n)$	Uniform color in the scene
[106]	KD[a]	$I^c(m,n)$	$O_r(m,n)$	Dichromatic model
[158]	KD[a]	$I^c(m,n)$ and $d_p(m,n)$	$O_r(m,n)$	Dichromatic model
[56]	KD[a]	$I^c(m,n)$	A_{tl}, $O_r(m,n)$	Depth from calibrated camera
[71]	KD[a]	$I^c(m,n)$	$\gamma(m,n)$ and $O_r(m,n)$	Transmission estimation utilizing mean texture
[134]	SI[b]	$I^c(m,n)$	A_{tl}, $\gamma(m,n)$ and $O_r(m,n)$	Brightest value assumption for A_{tl}; Contrast assumption
[42]	SI[b]	$I^c(m,n)$	A_{tl}, $\gamma(m,n)$ and $O_r(m,n)$	Shading and transmission are statistically uncorrelated
[58, 59]	SI[b]	$I^c(m,n)$	A_{tl}, $\gamma(m,n)$ and $O_r(m,n)$	At least one color channel has very low intensity
[137]	SI[b]	$I^c(m,n)$	A_{tl}, $\gamma(m,n)$ and $O_r(m,n)$	Maximal contrast assumption; Normalized A_{tl} is upper-bounded
[73, 108]	SI[b]	$I^c(m,n)$	$\gamma(m,n)$ and $O_r(m,n)$	$O_r(m,n)$ and A_{tl} are statistically independent
[3, 4]	SI[b]	$I^c(m,n)$	A_{tl} and $O_r(m,n)$	Grayworld colour constancy; Global contrast enhancement
[101]	SI[b]	$I^c(m,n)$	A_{tl}, $\gamma(m,n)$ and $O_r(m,n)$	Dark channel for $\gamma(m,n)$
[135]	SI[b]	$I^c(m,n)$	$\gamma(m,n)$, $O_r(m,n)$	Machine learning of $\gamma(m,n)$
[43]	SI[b]	$I^c(m,n)$	A_{tl}, $\gamma(m,n)$ and $O_r(m,n)$	Small image patch has uniform color and depth
[12]	SI[b]	$I^c(m,n)$	$\gamma(m,n)$ and $O_r(m,n)$	Learning of $\gamma(m,n)$ in neural network
[9]	SI[b]	$I^c(m,n)$	$\gamma(m,n)$ and $O_r(m,n)$	Non-local; finite color approximation

[a]Given restoration technique do not requires any kinds of mathematical.

[b]Given restoration technique requires a well-designed mathematical model to restore images

Index Metric (SSIM), Mean Squared Error (MSE), Absolute Mean Error (AME) Peak Signal to Noise Ratio (PSNR), etc. in literature.

6.1.1 Mean Square Error

The Mean square error (MSE) is a well-known quality metric used to estimate the error between the ground truth (G_t) and restored image (O_r). It lies between 0 to ∞. Close to 0 is required. It is computed as [2, 128]:

$$MSE = \frac{1}{R \times C} \sum_{n=1}^{R} \sum_{m=1}^{C} [G_t(i,j) - O_r(i,j)]^2 \tag{28}$$

$G_t(i,j)$ represents pixel intensities of ground truth image whereas $O_r(i,j)$ depicts the pixel value of restored image. Also m and n represents the pixel's coordinate values. R and C represents rows and columns, respectively.

6.1.2 Peak Signal to Noise Ratio

Peak signal to noise ratio (PSNR) evaluate the ratio of actual pixes value against the evaluated error using MSE. PSNR should be maximized. It is calculated as [2, 128]:

$$PSNR = 10 \log_{10} \left(\frac{255^2}{MSE} \right) \tag{29}$$

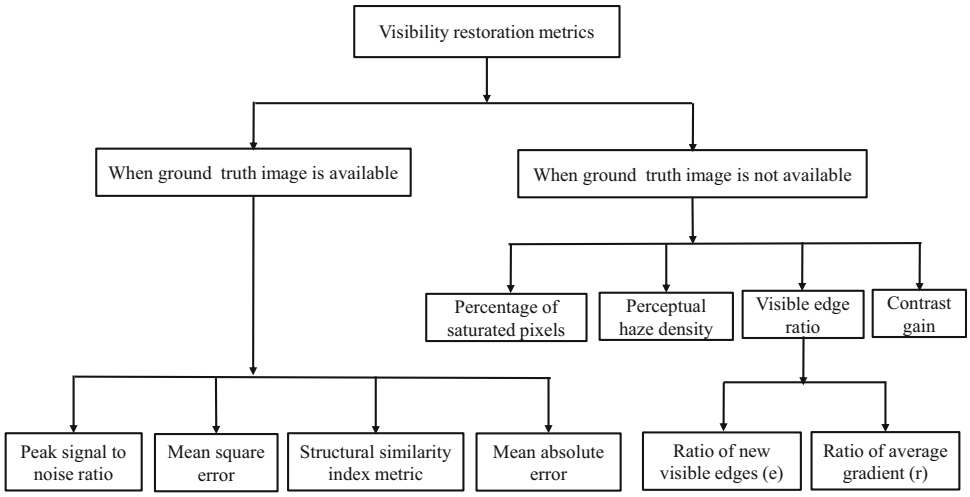

Fig. 4 Performance measures for dehazing techniques

6.1.3 Structural Similarity Index Metric

Structural similarity index metric (SSIM) evaluate the relationship of edges that has been neglected during PSNR calculation. SSIM $\in [0,1]$. Closer to 1 states higher structural quality of restored image. It is computed as [128]:

$$SSIM(m,n) = \left(\frac{2\mu_m\mu_n + c_1}{\mu_m^2 + \mu_n^2 + c_1}\right)\left(\frac{2\mu_{mj} + c_2}{\sigma_m^2 + \sigma_n^2 + c_2}\right) \tag{30}$$

Here, μ_m and μ_n are sample means of m and n, respectively. σ_m^2 and σ_n^2 are the sample variances of m and n, and σ_{mj} is the sample cross-covariance between m and n. Default values for c_1 and c_2 are 0.01 and 0.03.

6.1.4 Absolute Mean Error

The Absolute Mean Error (AME) is an error measure, which is utilized to evaluate the absolute difference between GT and OP produced by given restoration technique. It is basically a positive integer which ranges from 0 to 255 for a 8 bit image. Close to 0 is desired. AME can be computed as [2, 128]:

$$AME = \frac{1}{R \times C}\sum_{n=1}^{R}\sum_{m=1}^{C}\left|G_t(i,j) - O_r(i,j)\right| \tag{31}$$

6.2 When Ground Truth Images are not Available

In real-time applications, ground truth images are not available (also called blind-measures). It has been found that majority of researchers have used contrast gain, percentage of saturated pixels, visible edges ratio and perceptual haze density.

6.2.1 Contrast Gain

Contrast gain (C_g) is defined as the average contrast difference between hazy and restored image [138]. C_g needs to be maximum. It is computed as [126, 127]:

$$C_g = \Psi - \Phi \tag{32}$$

Here, Ψ and Φ are mean contrast values of I_s and O_r, respectively.

The mean contrast (A_c) is computed as:

$$A_c = \frac{1}{R \times C}\sum_{m=1}^{R}\sum_{n=1}^{M} C_t(i,j) \tag{33}$$

Here, C_t represents contrast of given image. It is computed by converting the color image into illumination channel.

6.2.2 Percentage of Saturated Pixels

C_g should not be so high that the pixels of restored image become saturated. Therefore, the Percentage of saturated pixels (ρ) is required to be evaluated [138]. ρ is computed as [126, 127]:

$$\rho = \frac{S_p}{R \times C} \tag{34}$$

Here, S_p shows the number of pixels that are saturated either black or white, which were not present in the hazy image. ρ should be minimum.

6.2.3 Visible Edges Ratio

Visible edges ratio is another measure that computes new visible edges (e) and ratio of average gradient ($\bar{r}$). The e

indicate the improved rate of visible edges after applying the dehazing technique. It needs to be maximized. It is computed as [57]:

$$e = \frac{n_k - n_l}{n_l} \tag{35}$$

where n_k and n_l depict the cardinal number of the visible edges in I_s and O_r, respectively.

The $\bar{r}$ considers the gradients of visible edges in the restored image, to show the restoration degree of the edges and texture detail. It should be maximized. $\bar{r}$ is computed as:

$$\bar{r} = e^{\left[\frac{1}{n_k}\sum_{m\in\phi_k} log r_m\right]} \tag{36}$$

Here, $r_m = \frac{\Delta_k}{\Delta_l}$, Δ_k and Δ_l are the gradients of Δ_k and Δ_l, respectively, r_m shows visible edges of O_r.

6.2.4 Perceptual Haze Density

Choi et al. designed a novel technique to predict the effect of haze in input image. In it, I_s is decomposed into $N \times N$ blocks and aggregated mean values are calculated. All $N \times N$ segments are implemented to estimate the haze aware characteristics like contrast, entropy, depth, variance, sharpness, saturation, colorfulness etc. Mahalanobis-like measure [139] is implemented on these characteristics to estimate the Multivariate Gaussian (MVG) fit of n dimensions is computed as:

$$P(s) = \frac{1}{\sqrt{(2\pi)^n |D|}} exp\left(-0.5 * (s-\mu)^t C^{-1}(s-\mu)\right) \tag{37}$$

where s denotes the haze aware statistical characteristics. μ shows mean and $n \times n$ indicate the covariance matrix of different hazy characteristics. D shows determinant and C^{-1} represents covariance matrix inverse for MVG. D and C^{-1} further derived using maximum likelihood (ML) estimation [35].

The Mahalanobis-like distance is computed as:

$$D = \sqrt{(m_1 - m_2)^t \left(\frac{C_1 + C_2}{2}\right)^{-1} (v_1 - v_2)} \tag{38}$$

where m_1 and m_2 are mean vectors. C_1 and C_2 are covariance matrices for MVG model of the restored corpus and MVG fit of the test image.

Another metric L_f which has restored level of the test hazy image is computed i.e., the distance norm of MVG versus hazy aware statistical characteristics. This information is obtained from a hazy test image and normal MVG model [23]. Afterwards, haze density (D) is computed as:

$$D_h = \frac{D}{1 + L_f} \tag{39}$$

Here, the values of D_h are proportional to the corresponding hazy density.

7 Comparative Analysis Based Upon Platform Used

Table 11 shows the comparison between some well-known dehazing techniques based upon hardware, Random access memory (RAM) and software required by restoration techniques along with their respective applications. It has been observed that restoration techniques do not require any specific processor or RAM to restore degraded images. Majority of existing researchers utilized MATLAB as a software for experimental purpose. It also shows that there exists no specific requirement of hardware or software for given restoration applications. Here, RAM represents random access memory. GPU and CUDA represent graphics processing unit and compute unified device architecture, respectively. FPGA denotes field-programmable gate array.

8 Significance and Benefits to Society

Dehazing techniques play an important role in computer vision applications. Figure 5 shows the most significant applications in which dehazing techniques are utilized as a pre-processing tool [81, 85, 157].

8.1 Remote Sensing

Remote sensing images are widely used for different areas ranging from mineral exploration to agricultural applications [136]. But, the poor quality of hyperspectral images will directly have an adverse effect on these applications [5]. Dehazing techniques are implemented on remote sensing image to attain a high-quality image [150].

8.2 Underwater Images

Underwater imaging often suffers from color sprinkle and color cast problems. Color sprinkle is produced by haze effects occurring when light imitated from scene is sprinkled multiple times by water particles. Therefore, underwater images generally have poor visibility [80]. Color cast is due to the fluctuating attenuation of light in dissimilar wavelengths, rendering underwater environments bluish. Therefore, color cast distorts the color of underwater images citeserikawa2014underwater,Vasamsetti201788,Ju2017180,Qureshi2017212. Therefore, dehazing

Table 11 Comparative analysis based upon hardware and software requirements

References	Technique	Hardware	RAM (GB)	Software	Applications
[166]	Region-wised medium transmission	Intel Core 2	4	MATLAB	Natural images
[17]	Edge collapse	Intel Core i5	16	MATLAB	Real images
[147]	Linear Transformation	Intel Core i7	8	MATLAB	Real images
[141]	Variational model	Intel Core Duo	2	MATLAB	Natural images
[143]	2D canonical correlation analysis	Xeon PC	4	MATLAB	Road transportation
[165]	Adaptive dark channel pripor	Intel Core i7	8	MATLAB	Natural images
[77]	Markov random field	Intel Core i5	8	C/C++	Stereo images
[142]	Multiscale retinex with color restoration	Intel Core i5	8	Xcode	Natural images
[28]	Weighted L_1-norm	Intel Core i5	4	C++	Natural images
[3]	Multiscale fusion	Intel Core i7	8	C/C++	Road and stereo images
[102]	Multiscale gradient	Intel Core i5	4	MATLAB	Rail and stereo images
[119]	Bright object handling	Intel Core i7	16	MATLAB	Stereo and natural images
[96]	DCP	Intel Core i5	8	MATLAB	Remote sensing imges
[82]	Histogram distribution prior	Intel Core i5	4	MATLAB	Underwater images
[49]	Negative correction	Intel Core i5	8	MATLAB	Road and stereo images
[146]	Region growing and Gaussian filter	Intel Core i7	8	MATLAB	Natural images
[90]	Local contrast	Intel Core 2	4	MATLAB	Natural images
[95]	Multiscale correlated wavelet	Intel Core i5	8	MATLAB	Natural images
[98]	Regression	Intel Core i5	8	MATLAB	Natural images
[112]	Deformed model	Intel Core i7	16	MATLAB	Remote sensing images
[66]	DCP	Intel Core i7	8	MATLAB	Aerial images
[174]	spatial-temporal coherence optimisation	Intel Core i5	4	OpenCV	Aerial images
[47]	Variational model	Intel Core i5	8	C/C++	Remote sensing images
[37]	region segmentation	Intel Core i2	4	C/C++	Underwater images
[63]	Fuzzy logic	Xeon E3-1231	16	CUDA	Natural images
[126]	Trilateral filter	Intel Core i5	8	MATLAB	Remote sensing images
[7]	DCP	FPGA	8	MATLAB	Natural videos
[93]	Bilateral filter	FPGA	2	C++	Natural images
[160]	DCP	GPU	4	CUDA	Natural images
[168]	DCP	FPGA	8	MATLAB	Real images
[169]	Virtual fusion method	GPU	8	CUDA C	Real images

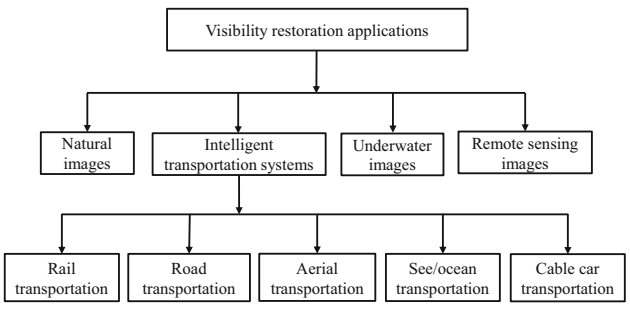

Fig. 5 Applications of dehazing techniques

techniques are required to remove the effect of color sprinkle and color cast from underwater images [117].

8.3 Intelligent Transportation Systems

Haze decreases the effective range of visual surveillance. This degradation is a spatially varying phenomena, which makes this problem non trivial. Dehazing is an essential technique in applications such as intelligent transportation system, vehicle detection, lane detection etc. [74, 175]. Following section describes some of the most popular applications of dehazing techniques to design an intelligent transpiration system.

8.3.1 Road Transportation

Many road accidents occur during hazy environment. Therefore, to reduce accident rate during hazy days it is

required to deliver haze free streaming to drivers. But, due to high speed of vehicles it is required to design a fast image dehazing technique [62].

8.3.2 Aerial Transportation

The takeoff and landing of airplanes become critical issue during hazy days. Many flights get delayed or some-times canceled due to poor visibility of runway and sky. Therefore, dehazing technique can be useful to handle this issue.

8.3.3 Rail Transportation

Even while train remains trashed of equipment because of poor weather conditions every year. The railways have not developed some fool-proof devices to mitigate this issue [25]. As the trains have presented technical advancement by adding fog safety devices on locomotives on a test foundation the device includes restricted function to ensure the locomotive pilots are advised effectively within time about another approaching signal and station [113]. Many trains get delay or sometimes even canceled due to hazy environment. Therefore, in order to handle this issue, one can use dehazing algorithms stream the clear scene for drivers [40].

8.3.4 Sea/Ocean Transportation

Sea fog that hinders visibility to less than one kilometer is considered a atmospheric hazard for traffic systems. It affects navigation of ships due to poor visibility and it can stop ship from moving along the ships channel. It can also be adverted and affect inland traffic systems. Future forecasts of sea fog are significant for reporting potential information to traffic system personal and the users of each system [68].

8.3.5 Cable Car Transportation

Cable car transportation is very popular in hillside areas. A cable car is any of a variety of cable transportation systems that depend on cables to pull vehicles along or lower them at a steady rate [8]. The cable cars are motor-less and engine-less. They are pulled by a cable that is rotated by a motor off-board. Many cable car get delay or sometimes even canceled due to heavy fog in the environment. To handle this issue, one can use dehazing techniques to stream visibility restored scene for cable car drivers.

9 Conclusion

In this paper, the existing dehazing techniques have reviewed form several perspectives such as theory, mathematical models, and performance measures. The review presented the strengths and weaknesses of different dehazing techniques. From the literature review, we are able to find out that each restoration technique seems to be suitable for certain weather conditions. This fact reveals that why the researchers try to combine different approaches into one technique. The review presented the basic concept behind the DCP based dehazing technique. This will be used as the basis for further study on restoration techniques. The review also identified the applications of restoration techniques. Some open issues and challenges have also presented that can inspire the future research in this area.

Compliance with Ethical Standards

Conflict of interest The authors declare that they have no conflict of interest.

References

1. Achanta R, Hemami S, Estrada F, Susstrunk S (2009) Frequency-tuned salient region detection. In: IEEE conference on computer vision and pattern recognition, 2009. CVPR 2009. IEEE, pp 1597–1604
2. Amintoosi M, Fathy M, Mozayani N (2011) Video enhancement through image registration based on structural similarity. Imaging Sci J 59(4):238–250
3. Ancuti CO, Ancuti C (2013) Single image dehazing by multi-scale fusion. IEEE Trans Image Process 22(8):3271–3282
4. Ancuti CO, Ancuti C, Bekaert P (2010) Effective single image dehazing by fusion. In: 17th IEEE international conference on image processing (ICIP), 2010. IEEE, pp 3541–3544
5. Ansari A, Danyali H, Helfroush MS (2017) Hs remote sensing image restoration using fusion with ms images by em algorithm. IET Signal Process 11(1):95–103
6. Bajić B, Lindblad J, Sladoje N (2016) Restoration of images degraded by signal-dependent noise based on energy minimization: an empirical study. J Electron Imaging 25(4):043,020
7. Bashir Z, Raja G, Ullah MO (2016) A video enhancement algorithm for low-lighting environment using field programmable gate array (fpga) architecture. NED Univ J Res 13(4):81
8. Beck A, Henneberger J, Schöpfer S, Fugal J, Lohmann U (2017) Hologondel: in situ cloud observations on a cable car in the swiss alps using a holographic imager. Atmos Meas Tech 10(2):459
9. Berman D, Avidan S et al (2016) Non-local image dehazing. In: Proceedings of the IEEE conference on computer vision and pattern recognition, pp 1674–1682
10. Buchsbaum G (1980) A spatial processor model for object colour perception. J Frankl Inst 310(1):1–26

11. Burt P, Adelson E (1983) The laplacian pyramid as a compact image code. IEEE Trans Commun 31(4):532–540
12. Cai B, Xu X, Jia K, Qing C, Tao D (2016) Dehazenet: an end-to-end system for single image haze removal. IEEE Trans Image Process 25(11):5187–5198
13. Caraffa L, Tarel JP (2012) Stereo reconstruction and contrast restoration in daytime fog. In: Asian conference on computer vision. Springer, pp 13–25
14. Carlevaris-Bianco N, Mohan A, Eustice RM (2010) Initial results in underwater single image dehazing. In: OCEANS 2010, IEEE, pp 1–8
15. Celik T, Li HC (2016) Residual spatial entropy-based image contrast enhancement and gradient-based relative contrast measurement. J Mod Opt 63(16):1600–1617
16. Chao L, Wang M (2010) Removal of water scattering. In: 2nd international conference on computer engineering and technology (ICCET), 2010. IEEE, vol 2, pp V2–35
17. Chen BH, Huang SC (2016) Edge collapse-based dehazing algorithm for visibility restoration in real scenes. J Disp Technol 12(9):964–970
18. Chen BH, Huang SC, Ye JH (2015) Hazy image restoration by bi-histogram modification. ACM Tran Intell Syst Technol TIST 6(4):50
19. Chen BH, Huang SC, Cheng FC (2016a) A high-efficiency and high-speed gain intervention refinement filter for haze removal. J Disp Technol 12(7):753–759
20. Chen C, Do MN, Wang J (2016) Robust image and video dehazing with visual artifact suppression via gradient residual minimization. In: European conference on computer vision. Springer, pp 576–591
21. Cheng FC, Cheng CC, Lin PH, Huang SC (2015) A hierarchical airlight estimation method for image fog removal. Eng Appl Artif Intell 43:27–34
22. Chiang JY, Chen YC (2012) Underwater image enhancement by wavelength compensation and dehazing. IEEE Trans Image Process 21(4):1756–1769
23. Choi LK, You J, Bovik AC (2015) Referenceless prediction of perceptual fog density and perceptual image defogging. IEEE Trans Image Process 24(11):3888–3901
24. Chuangbai X, Hongyu Z, Jing Y, Pu Y (2015) Traffic image defogging method based on wls. Infrared Laser Eng 3:052
25. Conca A, Ridella C, Sapori E (2016) A risk assessment for road transportation of dangerous goods: a routing solution. Transp Res Proc 14:2890–2899
26. Cong-Hua X, Wei-Wei Q, Xiu-Xiang Z, Feng Z (2016) Single image dehazing algorithm using wavelet decomposition and fast kernel regression model. J Electron Imaging 25(4):043,003
27. Crebolder JM, Sloan RB (2004) Determining the effects of eyewear fogging on visual task performance. Appl Ergon 35(4):371–381
28. Cui T, Tian J, Wang E, Tang Y (2016) Single image dehazing by latent region-segmentation based transmission estimation and weighted l 1-norm regularisation. IET Image Process 11(2):145–154
29. Ding M, Tong R (2013) Efficient dark channel based image dehazing using quadtrees. Sci China Inf Sci 56(9):1–9
30. Ding M, Wei L (2015) Single-image haze removal using the mean vector l2-norm of rgb image sample window. Optik Int J Light Electron Opt 126(23):3522–3528
31. Ding W, Li Y, Liu H (2016) Efficient vanishing point detection method in unstructured road environments based on dark channel prior. IET Comput Vis 10(8):852–860
32. Dou Z, Han Y, Sheng W, Ma X (2015) Image dehaze using alternating Laplacian and Beltrami regularizations. J Electron Imaging 24(2):023,004
33. Drews P, Nascimento E, Moraes F, Botelho S, Campos M (2013) Transmission estimation in underwater single images. In: Proceedings of the IEEE international conference on computer vision workshops, pp 825–830
34. Du Y, Guindon B, Cihlar J (2002) Haze detection and removal in high resolution satellite image with wavelet analysis. IEEE Trans Geosci Remote Sens 40(1):210–217
35. Duda RO, Hart PE, Stork DG (2012) Pattern classification. Wiley, Hoboken
36. El Khoury J, Le Moan S, Thomas JB, Mansouri A (2017) Color and sharpness assessment of single image dehazing. Multimedia tools and applications, pp 1–22
37. Emberton S, Chittka L, Cavallaro A (2018) Underwater image and video dehazing with pure haze region segmentation. Comput Vis Image Underst 168:145–156
38. Fan X, Wang Y, Tang X, Gao R, Luo Z (2016) Two-layer Gaussian process regression with example selection for image dehazing. IEEE Trans Circ Syst Video Technol PP(99):1
39. Fang F, Li F, Yang X, Shen C, Zhang G (2010) Single image dehazing and denoising with variational method. In: 2010 international conference on image analysis and signal processing (IASP). IEEE, pp 219–222
40. Fang K, Ke GY, Verma M (2017) A routing and scheduling approach to rail transportation of hazardous materials with demand due dates. Eur J Oper Res 261(1):154–168
41. Fang S, Shi Q, Cao Y (2013) Adaptive removal of real noise from a single image. J Electron Imaging 22(3):033,014
42. Fattal R (2008) Single image dehazing. ACM TOG 27(3):72
43. Fattal R (2014) Dehazing using color-lines. ACM TOG 34(1):13
44. Fu X, Wang J, Zeng D, Huang Y, Ding X (2015a) Remote sensing image enhancement using regularized-histogram equalization and dct. IEEE Geosci Remote Sens Lett 12(11):2301–2305
45. Fu Z, Yang Y, Shu C, Li Y, Wu H, Xu J (2015b) Improved single image dehazing using dark channel prior. J Syst Eng Electron 26(5):1070–1079
46. Galdran A, Pardo D, Picón A, Alvarez-Gila A (2015a) Automatic red-channel underwater image restoration. J Vis Commun Image Represent 26:132–145
47. Galdran A, Vazquez-Corral J, Pardo D, Bertalmío M (2015b) Enhanced variational image dehazing. SIAM J Imaging Sci 8(3):1519–1546
48. Galdran A, Vazquez-Corral J, Pardo D, Bertalmío M (2017) Fusion-based variational image dehazing. IEEE Signal Process Lett 24(2):151–155
49. Gao Y, Hu HM, Wang S, Li B (2014) A fast image dehazing algorithm based on negative correction. Signal Process 103:380–398
50. Ge G, Wei Z, Zhao J (2015) Fast single-image dehazing using linear transformation. Optik Int J Light Electron Opt 126(21):3245–3252
51. Ghani ASA, Isa NAM (2017) Automatic system for improving underwater image contrast and color through recursive adaptive histogram modification. Comput Electron Agric 141:181–195
52. Gibson KB, Nguyen TQ (2013) An analysis of single image defogging methods using a color ellipsoid framework. EURASIP J Image Video Process 1:37
53. Guan L (1995) Model-based neural evaluation and iterative gradient optimization in image restoration and statistical filtering. J Electron Imaging 4(4):407–413
54. Guo F, Peng H, Tang J (2016a) Genetic algorithm-based parameter selection approach to single image defogging. Inf Process Lett 116(10):595–602
55. Guo F, Peng H, Tang J (2016) Genetic algorithm-based parameter selection approach to single image defogging. Inf Process Lett 116(10):595–602

56. Hautière N, Tarel JP, Aubert D (2007) Towards fog-free in-vehicle vision systems through contrast restoration. In: IEEE conference on computer vision and pattern recognition, 2007. CVPR'07. IEEE, pp 1–8
57. Hautiere N, Tarel JP, Aubert D, Dumont E (2011) Blind contrast enhancement assessment by gradient ratioing at visible edges. Image Anal Stereol 27(2):87–95
58. He K, Sun J, Tang X (2011) X.: single image haze removal using dark channel prior. IEEE Trans Pattern Anal Mach Intell 33(12):2341–2353
59. He K, Sun J, Tang X (2011) Single image haze removal using dark channel prior. IEEE Trans Pattern Anal Mach Intell 33(12):2341–2353
60. He R, Wang Z, Fan Y, Feng DD (2015) Combined constraint for single image dehazing. Electron Lett 51(22):1776–1778
61. He S, Yang Q, Lau RW, Yang MH (2016) Fast weighted histograms for bilateral filtering and nearest neighbor searching. IEEE Trans Circ Syst Video Technol 26(5):891–902
62. Huang SC, Chen BH, Cheng YJ (2014) An efficient visibility enhancement algorithm for road scenes captured by intelligent transportation systems. IEEE Trans Intell Transp Syst 15(5):2321–2332
63. Hung CL, Yan RY, Wang HH (2016) Parallel image dehazing algorithm based on gpu using fuzzy system and hybird evolution algorithm. In: 2016 17th IEEE/ACIS international conference on software engineering, artificial intelligence, networking and parallel/distributed computing (SNPD). IEEE, pp 581–583
64. Jiang B, Meng H, Ma X, Wang L, Zhou Y, Xu P, Jiang S, Meng X (2017) Nighttime image dehazing with modified models of color transfer and guided image filter. Multimedia tools and applications, pp 1–17
65. Jiang G, Wong C, Lin S, Rahman M, Ren T, Kwok N, Shi H, Yu YH, Wu T (2015) Image contrast enhancement with brightness preservation using an optimal gamma correction and weighted sum approach. J Mod Opt 62(7):536–547
66. Jiang W, Ji M, Huang X, Wang C, Yang Y, Li T, Wang J, Zhang Y (2016) An improved dehazing algorithm of aerial high-definition image. In: Selected papers of the photoelectronic technology committee conferences held November 2015, international society for optics and photonics, vol 9796, p 97962T
67. Kawakami R, Zhao H, Tan RT, Ikeuchi K (2013) Camera spectral sensitivity and white balance estimation from sky images. Int J Comput Vis 105(3):187–204
68. Kennedy JP, Wilson JM (2017) Liabilities and responsibilities: ocean transportation intermediaries (otis) and the distribution of counterfeit goods. Marit Econ Logist 19(1):182–187
69. Khmag A, Al-Haddad S, Ramli AR, Kalantar B (2017) Single image dehazing using second-generation wavelet transforms and the mean vector l2-norm. The visual computer, pp 1–14
70. Kim JH, Jang WD, Sim JY, Kim CS (2013) Optimized contrast enhancement for real-time image and video dehazing. J Vis Commun Image Represent 24(3):410–425
71. Kopf J, Neubert B, Chen B, Cohen M, Cohen-Or D, Deussen O, Uyttendaele M, Lischinski D (2008) Deep photo: model-based photograph enhancement and viewing. ACM TOG 27:116
72. Koschmieder H (1938) Luftlicht und sichtweite. Naturwissenschaften 26(32):521–528
73. Kratz L, Nishino K (2009) Factorizing scene albedo and depth from a single foggy image. In: 2009 IEEE 12th international conference on computer vision. IEEE, pp 1701–1708
74. Kumar R, Kaushik BK, Balasubramanian R (2017) Fpga implementation of image dehazing algorithm for real time applications. In: Applications of digital image processing XL, international society for optics and photonics, vol 10396, p 1039633
75. Kumari A, Sahoo SK (2015) Fast single image and video deweathering using look-up-table approach. AEU Int J Electron Commun 69(12):1773–1782
76. Kwok N, Shi H, Fang G, Ha Q, Yu YH, Wu T, Li H, Nguyen T (2015) Color image enhancement using correlated intensity and saturation adjustments. J Mod Opt 62(13):1037–1047
77. Kwon O (2014) Single image dehazing based on hidden markov random field and expectation–maximisation. Electron Lett 50(20):1442–1444
78. Lee D, Lim S (2016) Improved structural similarity metric for the visible quality measurement of images. J Electron Imaging 25(6):063,015
79. Lee S, Yun S, Nam JH, Won CS, Jung SW (2016) A review on dark channel prior based image dehazing algorithms. EURASIP J Image Video Process 1:4
80. Li C, Guo J (2015) Underwater image enhancement by dehazing and color correction. J Electron Imaging 24(3):033,023
81. Li C, Guo J, Guo C, Cong R, Gong J (2017a) A hybrid method for underwater image correction. Pattern Recognit Lett 94:62–67
82. Li CY, Guo JC, Cong RM, Pang YW, Wang B (2016a) Underwater image enhancement by dehazing with minimum information loss and histogram distribution prior. IEEE Trans Image Process 25(12):5664–5677
83. Li J, Zhang H, Yuan D, Sun M (2015a) Single image dehazing using the change of detail prior. Neurocomputing 156:1–11
84. Li Y, Miao Q, Song J, Quan Y, Li W (2016b) Single image haze removal based on haze physical characteristics and adaptive sky region detection. Neurocomputing 182:221–234
85. Li Y, Zhang Y, Xu X, He L, Serikawa S, Kim H (2017) Dust removal from high turbid underwater images using convolutional neural networks. Opt Laser Technol. https://doi.org/10.1016/j.optlastec.2017.09.017
86. Li Z, Zheng J (2015) Edge-preserving decomposition-based single image haze removal. IEEE Trans Image Process 24(12):5432–5441
87. Li Z, Tan P, Tan RT, Zou D, Zhiying Zhou S, Cheong LF (2015b) Simultaneous video defogging and stereo reconstruction. In: Proceedings of the IEEE conference on computer vision and pattern recognition, pp 4988–4997
88. Li Z, Zheng J, Zhu Z, Yao W, Wu S (2015c) Weighted guided image filtering. IEEE Trans Image Process 24(1):120–129
89. Lian X, Pang Y, Yang A (2017) Learning intensity and detail mapping parameters for dehazing. Multimedia tools and applications, pp 1–26
90. Liao B, Yin P, Xiao C (2018) Efficient image dehazing using boundary conditions and local contrast. Comput Graph 70:242–250
91. Likhterov B, Kopeika NS (2004) Motion-blurred image restoration using modified inverse all-pole filters. J Electron Imaging 13(2):257–263
92. Liu H, Yang J, Wu Z, Zhang Q (2015) Fast single image dehazing based on image fusion. J Electron Imaging 24(1):013,020
93. Liu H, Huang D, Hou S, Pan X (2017) Nlarge size single image fast defogging and the real time video defogging fpga architecture. Neurocomputing 269:97–107
94. Liu S, Rahman MA, Wong CY, Lin CF, Wu H, Kwok N et al (2017) Image de-hazing from the perspective of noise filtering. Comput Electr Eng 62:345–359
95. Liu X, Zhang H, Ym Cheung, You X, Tang YY (2017b) Efficient single image dehazing and denoising: an efficient multi-scale correlated wavelet approach. Comput Vis Image Underst 162:23–33
96. Long J, Shi Z, Tang W, Zhang C (2014) Single remote sensing image dehazing. IEEE Geosci Remote Sens Lett 11(1):59–63

97. Lu H, Li Y, Nakashima S, Serikawa S (2016) Single image dehazing through improved atmospheric light estimation. Multimed Tools Appl 75(24):17,081–17,096
98. Luan Z, Shang Y, Zhou X, Shao Z, Guo G, Liu X (2017) Fast single image dehazing based on a regression model. Neurocomputing 245:10–22
99. Ma Z, Wen J, Zhang C, Liu Q, Yan D (2016) An effective fusion defogging approach for single sea fog image. Neurocomputing 173:1257–1267
100. McCartney EJ (1976) Optics of the atmosphere: scattering by molecules and particles. Wiley, New York, p 421
101. Meng G, Wang Y, Duan J, Xiang S, Pan C (2013) Efficient image dehazing with boundary constraint and contextual regularization. In: Proceedings of the IEEE international conference on computer vision, pp 617–624
102. Mi Z, Zhou H, Zheng Y, Wang M (2016) Single image dehazing via multi-scale gradient domain contrast enhancement. IET Image Process 10(3):206–214
103. Narasimhan SG, Nayar SK (2000) Chromatic framework for vision in bad weather. In: Proceedings of IEEE conference on computer vision and pattern recognition, 2000. IEEE, vol 1, pp 598–605
104. Narasimhan SG, Nayar SK (2002) Vision and the atmosphere. Int J Comput Vis 48(3):233–254
105. Narasimhan SG, Nayar SK (2003a) Contrast restoration of weather degraded images. IEEE Trans Pattern Anal Mach Intell 25(6):713–724
106. Narasimhan SG, Nayar SK (2003) Interactive (de) weathering of an image using physical models. In: IEEE workshop on color and photometric methods in computer vision, France, vol 6, p 1
107. Nayar SK, Narasimhan SG (1999) Vision in bad weather. In: The proceedings of the seventh IEEE international conference on computer vision, 1999. IEEE, vol 2, pp 820–827
108. Nishino K, Kratz L, Lombardi S (2012) Bayesian defogging. Int J Comput Vis 98(3):263–278
109. Nnolim UA (2017) Improved partial differential equation-based enhancement for underwater images using local–global contrast operators and fuzzy homomorphic processes. IET Image Process 11(11):1059–1067
110. Nnolim UA (2017b) Smoothing and enhancement algorithms for underwater images based on partial differential equations. J Electron Imaging 26(2):023,009
111. Oakley JP, Satherley BL (1998) Improving image quality in poor visibility conditions using a physical model for contrast degradation. IEEE Trans Image Process 7(2):167–179
112. Pan X, Xie F, Jiang Z, Yin J (2015) Haze removal for a single remote sensing image based on deformed haze imaging model. IEEE Signal Process Lett 22(10):1806–1810
113. Pellegrini P, Rodriguez J (2013) Single european sky and single european railway area: a system level analysis of air and rail transportation. Transp Res Part A Policy Pract 57:64–86
114. Peng YT, Cosman PC (2017) Underwater image restoration based on image blurriness and light absorption. IEEE Trans Image Process 26(4):1579–1594
115. Peng YT, Zhao X, Cosman PC (2015) Single underwater image enhancement using depth estimation based on blurriness. In: 2015 IEEE international conference on image processing (ICIP). IEEE, pp 4952–4956
116. Qiao X, Bao J, Zhang H, Zeng L, Li D (2017) Underwater image quality enhancement of sea cucumbers based on improved histogram equalization and wavelet transform. Inf Process Agric 4(3):206–213
117. Qing C, Yu F, Xu X, Huang W, Jin J (2016) Underwater video dehazing based on spatial–temporal information fusion. Multidimens Syst Signal Process 27(4):909–924
118. Qureshi MA, Beghdadi A, Deriche M (2017) Towards the design of a consistent image contrast enhancement evaluation measure. Signal Process Image Commun 58:212–227
119. Riaz I, Fan X, Shin H (2016a) Single image dehazing with bright object handling. IET Comput Vis 10(8):817–827
120. Riaz I, Yu T, Rehman Y, Shin H (2016b) Single image dehazing via reliability guided fusion. J Vis Commun Image Represent 40:85–97
121. Rong Z, Jun WL (2014) Improved wavelet transform algorithm for single image dehazing. Optik Int J Light Electron Opt 125(13):3064–3066
122. Schechner YY, Narasimhan SG, Nayar SK (2001) Instant dehazing of images using polarization. In: Proceedings of the 2001 IEEE computer society conference on computer vision and pattern recognition, 2001. CVPR 2001. IEEE, vol 1, p I
123. Serikawa S, Lu H (2014) Underwater image dehazing using joint trilateral filter. Comput Electr Eng 40(1):41–50
124. Shiau YH, Chen PY, Yang HY, Chen CH, Wang SS (2014) Weighted haze removal method with halo prevention. J Vis Commun Image Represent 25(2):445–453
125. Shwartz S, Namer E, Schechner YY (2006) Blind haze separation. In: 2006 IEEE computer society conference on computer vision and pattern recognition. IEEE, vol 2, pp 1984–1991
126. Singh D, Kumar V (2017a) Dehazing of remote sensing images using improved restoration model based dark channel prior. Imaging Sci J 65(5):1–11
127. Singh D, Kumar V (2017b) Modified gain intervention filter based dehazing technique. J Mod Opt 64(20):1–14
128. Singh D, Garg D, Singh Pannu H (2017) Efficient landsat image fusion using fuzzy and stationary discrete wavelet transform. Imaging Sci J 65(2):108–114
129. Song H, Gao Y, Chen Y (2014) Fast image dehazing using fuzzy system and hybrid evolutionary algorithm. In: Foundations and practical applications of cognitive systems and information processing. Springer, pp 275–283
130. Stanco F, Tenze L, Ramponi G (2005) Virtual restoration of vintage photographic prints affected by foxing and water blotches. J Electron Imaging 14(4):043,008
131. Sun W (2013) A new single-image fog removal algorithm based on physical model. Optik Int J Light Electron Opt 124(21):4770–4775
132. Sun W, Wang H, Sun C, Guo B, Jia W, Sun M (2015) Fast single image haze removal via local atmospheric light veil estimation. Comput Electr Eng 46:371–383
133. Tan H, He X, Wang Z, Liu G (2016) Parallel implementation and optimization of high definition video real-time dehazing. Multimedia tools and applications, pp 1–22
134. Tan RT (2008) Visibility in bad weather from a single image. In:. IEEE conference on computer vision and pattern recognition, 2008. CVPR 2008. IEEE, pp 1–8
135. Tang K, Yang J, Wang J (2014) Investigating haze-relevant features in a learning framework for image dehazing. In: Proceedings of the IEEE conference on computer vision and pattern recognition, pp 2995–3000
136. Tang X, Jiao L (2017) Fusion similarity-based reranking for sar image retrieval. IEEE Geosci Remote Sens Lett 14(2):242–246
137. Tarel JP, Hautiere N (2009) Fast visibility restoration from a single color or gray level image. In: 2009 IEEE 12th international conference on computer vision. IEEE, pp 2201–2208
138. Tripathi AK, Mukhopadhyay S (2012) Removal of fog from images: a review. IETE Tech Rev 29(2):148–156
139. Valls J, Aler R, Fernández Ó (2005) Using a mahalanobis-like distance to train radial basis neural networks. Computational intelligence and bioinspired systems, pp 504–510

140. Vasamsetti S, Mittal N, Neelapu BC, Sardana HK (2017) Wavelet based perspective on variational enhancement technique for underwater imagery. Ocean Eng 141:88–100
141. Wang D, Zhu J (2015) Fast smoothing technique with edge preservation for single image dehazing. IET Comput Vis 9(6):950–959
142. Wang J, He N, Lu K (2015) A new single image dehazing method with msrcr algorithm. In: Proceedings of the 7th international conference on internet multimedia computing and service, ACM, p 19
143. Wang L, Xiao L, Wei Z (2015b) Image dehazing using two-dimensional canonical correlation analysis. IET Comput Vis 9(6):903–913
144. Wang L, Xie W, Pei J (2015c) Patch-based dark channel prior dehazing for rs multi-spectral image. Chin J Electron 24(3):573–578
145. Wang R, Li R, Sun H (2016) Haze removal based on multiple scattering model with superpixel algorithm. Signal Process 127:24–36
146. Wang W, Yuan X, Wu X, Liu Y (2017a) Dehazing for images with large sky region. Neurocomputing 238:365–376
147. Wang W, Yuan X, Wu X, Liu Y (2017b) Fast image dehazing method based on linear transformation. IEEE Trans Multimed 19(6):1142–1155
148. Wang YK, Fan CT (2014) Single image defogging by multiscale depth fusion. IEEE Trans Image Process 23(11):4826–4837. https://doi.org/10.1109/TIP.2014.2358076
149. Wang Z, Feng Y (2014) Fast single haze image enhancement. Comput Electr Eng 40(3):785–795
150. Wei Q, Bioucas-Dias J, Dobigeon N, Tourneret JY, Chen M, Godsill S (2016) Multiband image fusion based on spectral unmixing. IEEE Trans Geosci Remote Sens 54(12):7236–7249
151. Wen H, Tian Y, Huang T, Gao W (2013) Single underwater image enhancement with a new optical model. In: 2013 IEEE international symposium on circuits and systems (ISCAS). IEEE, pp 753–756
152. Wong CY, Liu S, Liu SC, Rahman MA, Lin SCF, Jiang G, Kwok N, Shi H (2016) Image contrast enhancement using histogram equalization with maximum intensity coverage. J Mod Opt 63(16):1618–1629
153. Wong HS, Guan L (1998) Adaptive regularization in image restoration by unsupervised learning. J Electron Imaging 7(1):211–222
154. Wu F, Wang B, Yi X, Li M, Hao J, Qin H, Zhou H (2015) Visible and infrared image registration based on visual salient features. J Electron Imaging 24(5):053,017
155. Xie B, Guo F, Cai Z (2010) Improved single image dehazing using dark channel prior and multi-scale retinex. In: 2010 international conference on intelligent system design and engineering application (ISDEA). IEEE, vol 1, pp 848–851
156. Xie CH, Qiao WW, Liu Z, Ying WH (2016) Single image dehazing using kernel regression model and dark channel prior. Signal, image and video processing, pp 1–8
157. Xiong L, Li H, Xu L (2017) An enhancement method for color retinal images based on image formation model. Comput Methods Programs Biomed 143:137–150
158. Xu H, Guo J, Liu Q, Ye L (2012) Fast image dehazing using improved dark channel prior. In: 2012 IEEE international conference on information science and technology. IEEE, pp 663–667
159. Xu Y, Wen J, Fei L, Zhang Z (2016) Review of video and image defogging algorithms and related studies on image restoration and enhancement. IEEE Access 4:165–188
160. Xue Y, Ren J, Su H, Wen M, Zhang C (2013) Parallel implementation and optimization of haze removal using dark channel prior based on cuda. In: High performance computing. Springer, pp 99–109
161. Yang HY, Chen PY, Huang CC, Zhuang YZ, Shiau YH (2011) Low complexity underwater image enhancement based on dark channel prior. In: 2011 second international conference on innovations in bio-inspired computing and applications (IBICA). IEEE, pp 17–20
162. Yang Y, Sun X, Yang H, Li CT (2008) Removable visible image watermarking algorithm in the discrete cosine transform domain. J Electron Imaging 17(3):033,008
163. Yang Y, Fu Z, Li X, Shu C, Li X (2013) A novel single image dehazing method. In: 2013 international conference on computational problem-solving (ICCP). IEEE, pp 275–278
164. Yoon SM (2016) Visibility enhancement of fog-degraded image using adaptive total variation minimisation. Imaging Sci J 64(2):82–86
165. Yu T, Riaz I, Piao J, Shin H (2015) Real-time single image dehazing using block-to-pixel interpolation and adaptive dark channel prior. IET Image Process 9(9):725–734
166. Yuan H, Liu C, Guo Z, Sun Z (2017) A region-wised medium transmission based image dehazing method. IEEE Access 5:1735–1742
167. Zeng L, Dai Y (2016) Single image dehazing based on combining dark channel prior and scene radiance constraint. Chin J Electron 25(6):1114–1120
168. Zhang B, Zhao J (2017) Hardware implementation for real-time haze removal. IEEE Trans VLSI Syst 25(3):1188–1192
169. Zhang J, Hu S (2014) A gpu-accelerated real-time single image de-hazing method using pixel-level optimal de-hazing criterion. J Real Time Image Process 9(4):661–672
170. Zhang W, Hou X (2017) Estimation algorithm of atmospheric light based on ant colony optimization. In: Proceedings of the 2017 international conference on intelligent systems, metaheuristics & swarm intelligence, ACM, pp 20–25
171. Zhang W, Liang J, Ju H, Ren L, Qu E, Wu Z (2017) Study of visibility enhancement of hazy images based on dark channel prior in polarimetric imaging. Optik Int J Light Electron Opt 130:123–130
172. Zhao H, Xiao C, Yu J, Xu X (2015a) Single image fog removal based on local extrema. IEEE/CAA J Autom Sin 2(2):158–165
173. Zhao X, Jin T, Qu S (2015b) Deriving inherent optical properties from background color and underwater image enhancement. Ocean Eng 94:163–172
174. Zhao X, Ding W, Liu C, Li H (2017) Haze removal for uav aerial video based on optimization of spatial-temporal coherence. IET Image Process 12(1):88–97
175. Zheng L, Shi H, Gu M (2017) Infrared traffic image enhancement algorithm based on dark channel prior and gamma correction. Mod Phys Lett B:1740044
176. Zheng N, Loizou G, Jiang X, Lan X, Li X (2007) Computer vision and pattern recognition. Int J Comput Math 84(9):1265–1266
177. Zhu Q, Mai J, Shao L (2015) A fast single image haze removal algorithm using color attenuation prior. IEEE Trans Image Process 24(11):3522–3533